



# Simulation of gel phase formation and melting in lipid bilayers using a coarse grained model

Siewert J. Marrink\*, Jelger Risselada, Alan E. Mark

*Department of Biophysical Chemistry, University of Groningen, Nijenborgh 4, 9747 AG Groningen, The Netherlands*

Received 14 October 2004; received in revised form 8 March 2005; accepted 8 March 2005

Available online 28 March 2005

## Abstract

The transformation between a gel and a fluid phase in dipalmitoyl-phosphatidylcholine (DPPC) bilayers has been simulated using a coarse grained (CG) model by cooling bilayer patches composed of up to 8000 lipids. The critical step in the transformation process is the nucleation of a gel cluster consisting of 20–80 lipids, spanning both monolayers. After the formation of the critical cluster, a fast growth regime is entered. Growth slows when multiple gel domains start interacting, forming a percolating network. Long-lived fluid domains remain trapped and can be metastable on a microsecond time scale. From the temperature dependence of the rate of cluster growth, the line tension of the fluid–gel interface was estimated to be  $3 \pm 2$  pN. The reverse process is observed when heating the gel phase. No evidence is found for a hexatic phase as an intermediate stage of melting. The hysteresis observed in the freezing and melting transformation is found to depend both on the system size and on the time scale of the simulation. Extrapolating to macroscopic length and time scales, the transition temperature for heating and cooling converges to  $295 \pm 5$  K, in semi-quantitative agreement with the experimental value for DPPC (315 K). The phase transformation is associated with a drop in lateral mobility of the lipids by two orders of magnitude, and an increase in the rotational correlation time of the same order of magnitude. The lipid headgroups, however, remain fluid. These observations are in agreement with experimental findings, and show that the nature of the ordered phase obtained with the CG model is indeed a gel rather than a crystalline phase. Simulations performed at different levels of hydration furthermore show that the gel phase is stabilized at low hydration. A simulation of a small DPPC vesicle reveals that curvature has the opposite effect.

© 2005 Elsevier Ireland Ltd. All rights reserved.

**Keywords:** Main phase transition; Molecular dynamics; Nucleation and growth; Heterophase fluctuations; Hexatic phase; Membrane; DPPC; Order–disorder

## 1. Introduction

Recently, we introduced a coarse grained (CG) model for simulations of lipid systems (Marrink et al., 2004). Although primarily parametrized to represent lipid membranes in the fluid phase, it was shown that

\* Corresponding author. Tel.: +31 50 3634339;  
fax: +31 50 3634800.

E-mail address: [s.j.marrink@rug.nl](mailto:s.j.marrink@rug.nl) (S.J. Marrink).

an ordered phase is formed when cooled. Ordered domains in lipid membranes are believed to be of biological importance, and much experimental effort is devoted to the study of raft and gel domain formation in model lipid systems. The gel phase differs from the fluid or liquid-crystalline  $L_\alpha$  phase by a number of key features (Koynova and Caffrey, 1998; Nagle and Tristram-Nagle, 2000): (i) the area per lipid is lower; (ii) the lipid tails are almost fully extended with few gauche defects remaining; (iii) the lipids are hexagonally ordered; and (iv) the lateral mobility is strongly reduced. The difference between the tilted  $L_{\beta'}$  and untilted  $L_\beta$  gel phase is the presence of an average tilt of the lipid tails with respect to the bilayer normal. At even lower temperatures, most phospholipids adopt a crystal phase with the lipids packed in an (presumably) orthorhombic rather than hexagonal lattice (Koynova and Caffrey, 1998). In the crystal phase, the lipids are fully ordered and virtually immobile. Various metastable long living subgel phases are found in between the crystal and gel phases.

Here, we present a detailed molecular dynamics (MD) simulation study of the formation of the untilted  $L_\beta$  gel phase in a CG lipid membrane. Although the lipid modeled, dipalmitoyl-phosphatidylcholine (DPPC), experimentally forms a tilted gel phase, such tilt is not observed with the CG model. This is a direct consequence of the coarse graining procedure which implicitly incorporates some of the tail entropy of the lipid tails into the volume of the CG interaction sites. Tilt can be induced by changing the volume of the tails sites. However, the titled gel phase is less relevant to biological processes. In this study, we focus on the transformation between the  $L_\alpha$  and  $L_\beta$  phases. Our aims are two-fold: (i) to test the applicability of the CG model when modeling ordered lipid phases; and (ii) to provide insight into the molecular details of the lipid order–disorder transformation on a nanosecond time and a nanometer length scale.

There has been a lot of confusion in the general biophysical literature regarding the relationship of the kinetic versus the equilibrium aspects of phase transitions. In the fields of statistical mechanics, the terms ‘phase transformation’ and ‘phase transition’ have distinct meanings which we will adopt in the current paper. Phase transformation is used to describe the process of conversion from one phase to another; this includes kinetic aspects and the identification of interme-

diates, such as those associated with the nucleation and growth mechanism. The process of phase transformation is studied by driving an initial phase into a region of the phase diagram where it is metastable or unstable. Hysteresis is usually observed during phase transformation. Phase transition refers to the equilibrium phase diagram.

According to two-dimensional nucleation theory (e.g. Abraham, 1974; Kashchiev, 2000), the transformation from a disordered to an ordered phase requires the formation of a so-called critical nucleus, or gel domain when we consider lipid bilayers. The free energy  $\Delta G$  to form a gel domain in the fluid phase is given by the expression

$$\Delta G = \Delta\mu n + 2\gamma[\pi\sigma n]^{1/2} \quad (1)$$

where  $\Delta\mu$  denotes the chemical potential of a lipid in the gel with respect to the fluid phase,  $\gamma$  the line tension between the fluid and gel phase,  $n$  the amount of lipids constituting the nucleus, and  $\sigma$  the area per lipid in the gel phase. Above the main phase transition temperature, both terms are positive and only small nuclei can form (so-called heterophase fluctuations (Frenkel, 1946; Kharakoz and Shlyapnikova, 2000)). Below the transition temperature, the chemical potential in the gel phase becomes lower than that of a lipid in the fluid phase, driving the transformation. However, this driving force is opposed by the line tension arising from the gel–fluid interface. There exists a critical nucleus size  $n^*$

$$n^* = \frac{\pi\sigma\gamma^2}{\Delta\mu^2} \quad (2)$$

for which the free energy exhibits a maximum  $\Delta G^*$

$$\Delta G^* = \frac{\pi\sigma\gamma^2}{\Delta\mu} \quad (3)$$

Gel nuclei with a size  $n < n^*$  are unstable and will dissipate. Nuclei with  $n > n^*$ , however, will grow thereby transforming the entire system into the state of lower free energy, i.e. the gel. The time  $t^*$  required to overcome this barrier will scale as

$$t^* \propto \exp \frac{\Delta G^*}{kT} \quad (4)$$

For a system quenched to a temperature much lower than the transition temperature,  $\Delta\mu$  becomes large and  $\Delta G^*$  vanishingly small. In this case, there is almost

no impediment to the phase transformation process. On the other hand, at a temperature close to the phase transition temperature, both the critical cluster size and the time required to form the critical cluster diverge. If cluster growth results from the (reversible) addition of single lipids to the cluster boundary, the speed of gel phase propagation is given by (Kharakoz and Shlyapnikova, 2000)

$$u = u_{\max} \left( 1 - \exp \frac{\Delta\mu}{kT} \right) \quad (5)$$

where  $u_{\max}$  denotes the maximum achievable speed when the probability of the reverse process can be neglected. Direct experimental evidence for the nucleation and growth mechanism in lipid bilayers is hard to obtain. Within the framework of heterophase fluctuations, Kharakoz and Shlyapnikova (2000) were able to derive a kinetic model explaining the ultrasonic anomalies observed in experiments on multilamellar vesicles. By fitting to the kinetic model, estimates of the line tension and the thermodynamic driving force could be obtained. Direct visualization of the initial stages of cluster nucleation and growth has thus far only been achieved for two-dimensional colloidal systems. Very good agreement with the classical two-dimensional nucleation theory was recently reported for colloidal nucleation driven by an electric field, which allowed precise control over the thermodynamic driving force (Zhang and Liu, 2004).

Whereas the formation of a solid phase from a liquid can be described by nucleation theory, the reverse process is usually described in terms of defect growth. Theoretical arguments (Kosterlitz and Thouless, 1973; Halperin and Nelson, 1978) predict that the transition between a solid (crystal) and liquid state in two dimensions involves a so-called hexatic phase which is intermediate between the two. The hexatic phase is characterized by the presence of defects called dislocations which destroy the long-range translational order while preserving a quasi-long-range orientational order. Whether or not the gel phase of lipid bilayers is hexatic in nature is still an open question. Experimental evidence has been presented by Smith et al. (1990), characterizing the lateral correlation in the gel phase of DMPC (myristoyl tails) as relatively short-ranged ( $\sim 20$  nm) suggesting a hexatic phase. Sun et al. (1994), in contrast, report that order in the gel phase of DPPC

persists over length scales greater than 290 nm. Analysis of an experimental two-dimensional model system consisting of microspheres (Quinn and Goree, 2001) reveals that even though translational and orientational correlation functions are in agreement with the theoretical predictions, the underlying structure is not. An alternative theory of two-dimensional melting (Chui, 1983) predicts melting to occur through the spontaneous generation of grain boundaries. This would give rise to the same type of correlational behavior without, however, the occurrence of an intermediate hexatic phase.

In order to test the predictions of the theoretical models concerning the phase transformation process in lipid bilayers, computer simulations are an appropriate tool. Using atomistic models, the liquid-crystalline phase has been studied extensively using MD (Tieleman et al., 1997). The gel phase has only been studied in a few MD studies, all based on pre-constructed bilayers (Essmann et al., 1995; Tu et al., 1996; Venable et al., 2000). The spontaneous formation of a gel phase has not been extensively studied in atomistic detail as yet. An exception is the recent observation of the spontaneous formation of a ripple phase in DPPC bilayers when cooled (de Vries et al., *in press*). Coarse grained models, where some of the internal degrees of freedom are eliminated, offer an opportunity to study the phase behavior and transformation processes in a way not yet possible in atomic detail. CG simulations of gel formation in lipid bilayers have been reported recently by Kranenburg et al. (2003), Brannigan et al. (2004) and Stevens (2004). Kranenburg et al. used dissipative particle dynamics to study qualitatively the phase behavior of coarse grained amphiphilic systems. For lipid-like molecules, a chain ordering phase transformation was observed at low temperature. The ordered phase was found to be either interdigitated or tilted depending on the composition of the lipid headgroup. No attempt was made to distinguish between a gel or crystal phase. Brannigan et al. used a Monte Carlo scheme to study the phase behavior of highly simplified bilayers, consisting of spherocylinders representing lipid molecules. Both a liquid phase (characterized by a large area per lipid and high mobility) and an ordered phase (small area, reduced mobility) were identified for this model. Based on a small regime with apparent intermediate mobility, the authors speculated about the possible existence of a hexatic phase.

Stevens reported MD simulations of the temperature dependence of a CG lipid model adopted from a polymer model. A low temperature, tilted, gel phase was found. A strong hysteresis was noted between the melting and freezing temperature of the model, attributed to kinetic trapping. Unfortunately, none of the studies cited above have reported any details about the phase transformation process itself.

Here, we use our recently developed coarse grained lipid model (Marrink et al., 2004) to simulate the order–disorder phase transformation in lipid membranes using the MD technique. Although the current CG model was optimized for the liquid-crystalline phase, previously it was shown that cooling of a 256 lipid DPPC patch below a temperature of 270 K results in the formation of an ordered phase, resembling an untilted gel phase (Marrink et al., 2004). Also in lipid mixtures consisting of DLPC and DSPC (lauroyl and stearyl tails, respectively), using the same CG model, the formation of an ordered phase was observed (Faller and Marrink, 2004). Based on the decay of the rotational correlation function and the lateral mobility of the lipids, it was concluded that the ordered phase was gel-like rather than crystalline. The questions that we aim to address in the current paper are: By what mechanism does the phase transformation occur? Is it possible to determine the phase transition temperature? How important are finite size effects? Can tilt be reproduced by the model? Is the ordered phase a true gel phase, a crystalline phase or perhaps a hexatic phase?

The remainder of this paper is organized as follows. Section 2 provides details about the CG lipid model, the simulation procedure, and the tools used for analysis. The results are divided into a number of subsections. First, the general phase transformation pathway is shown, focussing on the transformation from the liquid to ordered state followed by a more condensed section on the reverse process. Second, the effect of finite size and finite simulation length on the phase transition temperature observed is evaluated. The effect of the hydration level and curvature on the transition temperature is also investigated. The third subsection shows that the low temperature ordered phase is a gel as opposed to a crystalline phase, and illustrates how the CG model can be parametrized to obtain a tilted rather than an untilted gel phase. Discussion of the results is embedded within each of these sections. Finally, the main conclusions are summarized.

## 2. Methods

### 2.1. Coarse grained lipid model

In the coarse grained model, which is based on the pioneering work of Smit et al. (1990), small groups of atoms (four to six heavy atoms) are united into single interaction centers. All particles interact through pairwise short-range Lennard–Jones (LJ) potentials. The strength of the interaction depends on the nature of the particles. The particles differ in their degree of hydrophilicity. Hydrophilic particles are attracted more strongly to other hydrophilic particles than to hydrophobic particles. Fig. 1 shows the coarse grained representation of the DPPC lipid used in this study. In the coarse grained representation, the PC headgroup consists of two hydrophilic groups, one for the choline and one for the phosphate group. Two sites of intermediate hydrophilicity are used to represent the glycerol ester moiety. Each of the lipid tails is modeled by 4 hydrophobic particles, representing 16 methylene/methyl units. The solvent is modeled by individual hydrophilic particles each representing four ‘real’ water molecules. In addition to the LJ interactions, a screened Coulombic interaction is used to model the electrostatic interaction between the zwitterionic headgroups. Bonded interactions are modeled by a weak harmonic potential. Harmonic angle potentials provide the appropriate stiffness for the molecules. The force constant of the angle potentials are weak ( $25 \text{ kJ mol}^{-1}$ ), allowing deviations of  $25^\circ$  at the cost of  $kT$ . All of the tail angle potentials have an equilibrium value of  $180^\circ$ . Full details of the coarse grained force field can be found in a previous publication (Marrink et al., 2004) and at our website <http://md.chem.rug.nl/~marrink/coarsegrain.html>. The CG model reproduces many of the structural, dynamic, and elastic properties of both lamellar and non-lamellar states of a variety of phospholipids (Marrink et al., 2004).

### 2.2. Simulation procedure

In order to estimate the transition temperature, two sets of simulations were performed. The first set (‘cooling’) consists of simulations of bilayer patches starting from an equilibrated liquid-crystalline configuration (at  $T = 325 \text{ K}$ ) which were then cooled instantaneously to a given (lower) target temperature. The target tempera-

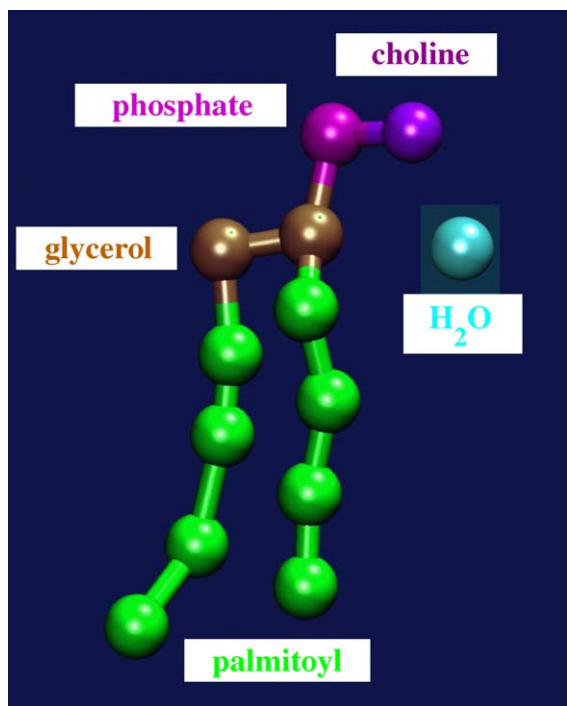


Fig. 1. Coarse grained representation of DPPC. The choline and phosphate moieties are both modeled by a hydrophilic particle bearing a positive and negative charge, respectively. Each of the palmitoyl tails is modeled by four hydrophobic particles. The glycerol ester backbone is modeled by two particles of intermediate hydrophilicity. The water particle is hydrophilic, representing four real water molecules. The molecule is kept together by harmonic bond potentials. Angle potentials provide the appropriate stiffness for the lipid tails.

ture was varied systematically to determine the range in temperature for which the transformation to a gel phase was observed. The second set of simulations (‘heating’) employed the opposite procedure, i.e. instantaneous heating starting from a gel phase. To study the effect of system size on the transition temperature, both sets of simulations were performed on bilayer patches of 128, 512, and 2048 lipids, in the temperature range 270–325 K. The simulations of the largest patches (2048 lipids) were also used to study the kinetics of the transformation process in detail. Additional simulations on even larger patches of 8192 lipids were performed to study long-range order and the possible existence of a hexatic phase. These simulations were started from a defect-free, perfectly ordered gel patch which was ob-

tained from lateral copying of a very small patch (64 lipids) equilibrated at low temperature during a multi-microsecond simulation.

The amount of water in all systems was 32 water molecules/lipid, close to the swelling limit of DPPC in the  $L_{\alpha}$  phase (30.1 water molecules/lipid at 325 K; Nagle and Tristram-Nagle, 2000). Note, one aspect of the simulations not fully consistent with experiment is the fixed water/lipid ratio. The experimental swelling limit for the fluid phase differs considerably from that of the gel phase (12.6 water molecules/lipid for DPPC at 293 K; Nagle and Tristram-Nagle, 2000). In the simulations, the size of the system is too small for the water to be able to phase separate. Therefore, the hydration level remains constant. A separate series of cooling simulations of a 128 lipid bilayer patch with a reduced amount of water (down to 4 water molecules/lipid) was performed to study the effect of the hydration level on the transition temperature. To investigate the role of curvature, a small vesicle was also simulated. The vesicle was obtained by taking a fluid bilayer consisting of 2568 lipids, adding excess water in the lateral directions (total amount of CG water: 88,100), and letting the bilayer spontaneously encapsulate water until a vesicle was formed. This procedure is the same one as described in Marrink and Mark (2003). The vesicle was subsequently quenched to different temperatures below the estimated transition temperature.

All systems were coupled to standard heat and pressure baths (Berendsen et al., 1984) to maintain constant temperature and pressure throughout the simulations. The pressure of the lamellar systems was coupled anisotropically, i.e. independently in all directions at a value of 1 bar. This corresponds to zero surface tension conditions. For correct computation of the lateral diffusion coefficient of the lipids, the center-of-mass motion per monolayer was removed at each step during the simulations. The box shape was fully flexible (triclinic) in order to allow for the development of hexagonal chain packing in the gel phase. The vesicular system was coupled isotropically (1 bar) using a cubic box. Periodic boundary conditions are applied to all systems. Simulations were performed with the Gromacs simulation software (Lindahl et al., 2001).

The total simulation time for each of the systems varied between 1 and 20  $\mu$ s, depending on the system size and the time required to reach an equilibrium state. In general, the systems containing 128 lipids were run for

10  $\mu\text{s}$ , systems containing 512 lipids for 5  $\mu\text{s}$ , and systems containing 2048 or 8192 lipids for 1  $\mu\text{s}$ . The systems containing the vesicle were simulated for 0.5  $\mu\text{s}$ . The time scale used in this paper is an effective time scale. It is four times larger than the actual simulation time. The effective time scale for the CG model has been determined by relating the diffusion rate of the solvent to the experimental self-diffusion rate of bulk water and validated by examining other experimentally accessible dynamical properties, such as the lipid lateral diffusion rates in bilayers and the permeation rate of water across a bilayer all of which were reproduced at a semi-quantitative level (Marrink et al., 2004).

### 2.3. Cluster analysis

In order to determine lipid coordination numbers, a Voronoi analysis was performed on the trajectories using the Triangle program (Shewchuk, 2002). The Voronoi cells were computed using the positions of the C2 tail sites (see Fig. 1) in each of the monolayers separately. From the Voronoi cells, the number of neighbors of a C2 site can be determined. The Voronoi analysis was used to identify lattice defects such as five- and seven-fold disclinations (i.e. lipids having five or seven neighbors). The Voronoi analysis was also used to distinguish lipids in the fluid from lipids in the gel phase. A lipid tail is considered to be in the gel phase if: (i) the C2 site of the tail has exactly six neighbors; and (ii) at least five of these neighbors lie within a distance smaller than a cut-off distance  $D_{\text{cut}}^a = 0.75$  nm.  $D_{\text{cut}}^a$  corresponds to the distance of the first minimum of the radial pair distribution function  $g(r)$  of the C2 tail beads in the gel phase. The first selection criterium selects all lipid tails which have a six-fold coordination number, a prerequisite for the gel phase. The second selection criterium filters out the tails in the fluid state which are also six-coordinated from time to time, however, deviating considerably from a perfect hexagon. A straightforward cluster algorithm was subsequently applied to connect the gel lipids into gel clusters. Here, a second cut-off distance was used,  $D_{\text{cut}}^b = 0.51$ , corresponding to the distance of the maximum of the first neighbor peak of  $g(r)$ . Two lipid gel tails belong to the same cluster if the lateral distance lies within the cut-off distance  $D_{\text{cut}}^b$ . The cluster size in terms of number of lipids is obtained simply by counting the amount of C2 sites present in the cluster, divided by two. The se-

lection criteria used to define gel clusters are inevitably somewhat arbitrary. Different combinations of cut-off distances and number of neighbors were tested. Within reasonable limits, different criteria led to clusters of similar composition and size. The results which are based on the cluster analysis are not very sensitive to the exact definition.

From the cluster analysis, two time-dependent functions are derived:  $n^{\text{total}}(t)$  which is the sum over all gel clusters present at time  $t$ , and  $n^{\text{max}}(t)$  which denotes the largest cluster present at time  $t$ . The functions are used to calculate the critical time, size, and growth rate of the gel clusters. The critical time,  $t^*$ , which represents the time required for the quenched fluid phase to nucleate a gel cluster large enough to overcome the line tension (Eq. (4)) was estimated at the point where  $n^{\text{max}}(t)$  starts increasing irreversibly. The critical cluster size,  $n^*$ , was obtained from the maximum of the function  $n^{\text{max}}(t)$  over the interval  $0 < t < t^*$ , thus representing the largest gel cluster that can be formed which is not stable. The linear growth rate  $u$  of the clusters was obtained from

$$u = \frac{dR}{dt} = \frac{\sigma}{\pi} \frac{d\sqrt{(n^{\text{total}})}}{dt} \quad (6)$$

where  $R$  denotes the average radius of the growing clusters.

Based on the temperature dependence of the gel nucleation process, the formation rate and critical size of the gel clusters can be used to obtain the line tension and the entropy characterizing the phase transformation. Assuming that the enthalpy and entropy of lipids in both the gel and the fluid phase are temperature independent over a temperature interval  $\Delta T = T_m - T$  (where  $T_m$  is the transition temperature), it follows that the driving potential

$$\Delta\mu = \Delta s \Delta T \quad (7)$$

where  $\Delta s$  denotes the entropy of a lipid in the gel phase with respect to the fluid phase. Combining Eqs. (3), (4) and (7), it follows that a plot of  $\ln t^*$  versus  $1/\Delta T$  gives a straight line with slope  $\gamma^2 \pi \sigma / \Delta s k T$ . A plot of the critical cluster radius  $R^* = \sqrt{n^*} \sigma / \pi$  versus  $1/\Delta T$ , using Eqs. (2) and (7), also gives a straight line with slope  $\gamma \sigma / \Delta s$ . Simultaneous fitting of the scaling of the critical time and cluster size with the inverse temperature drop allows for the determination of both the line tension and the entropy difference. For small  $\Delta s \Delta T / k T$ , the clus-

ter growth rate is expected to increase linearly with the temperature interval, following  $u \simeq -u_{\max} \Delta s \Delta T / kT$  (combining Eqs. (5) and (7)).

### 3. Results and discussion

#### 3.1. Liquid–gel transformation

##### 3.1.1. Transformation process

Figs. 2 and 3 show the time evolution of a 2048 DPPC bilayer patch quenched from  $T = 325$  to 283 K. These figures represent one particular time series only, however, the qualitative features are illustrative of the transformation process observed in general as will be discussed in more detail further on. In Fig. 2, a cut through the bilayer is shown at full resolution, revealing the tail ordering, whereas in Fig. 3, only the C2 tail beads of the lipids are shown, viewed from above. Before the quench, at  $T = 325$  K, the bilayer is in the  $L_{\alpha}$  phase, characterized by disordered lipid tails, fast lateral diffusion, and the absence of long-range lateral order. Within a few nanoseconds after the quench to  $T = 283$  K, the bilayer relaxes to a state characterized by increased lipid tail order and a concomitant decrease in lipid area. It is nevertheless still liquid (see snapshot at  $t = 0$  ns in Fig. 2). Note that here, and in the remainder of this paper, time  $t = 0$  corresponds to the time point immediately after the initial relaxation process. The area/lipid relaxes from 0.64 to 0.56 nm<sup>2</sup>. Experimentally, the area/lipid for DPPC is 0.64 nm<sup>2</sup> at  $T = 325$  K (Nagle and Tristram-Nagle, 2000) and 0.67 nm<sup>2</sup> at  $T = 338$  K (Petrache et al., 2000). A linear extrapolation of the experimental temperature dependence to a temperature of  $T = 283$  predicts an area/lipid of 0.55 nm<sup>2</sup> for the supercooled  $L_{\alpha}$  phase, close to what is obtained with the CG model. Soon after the initial relaxation, small gel domains form spontaneously (snapshot at  $t = 1$  ns in Fig. 3). These small gel domains, consisting typically of 10–20 lipids, are metastable and quickly disappear after their formation. After 25 ns, however, a small ordered domain is seen to have formed that remains stable. This domain involves both monolayers, involving 30–40 lipids per monolayer. Subsequently, this domain grows rapidly (snapshots at  $t = 50$ –75 ns) until at  $\sim 100$  ns the gel domains have percolated in both lateral directions. A few fluid domains now remain, trapped by the gel ma-

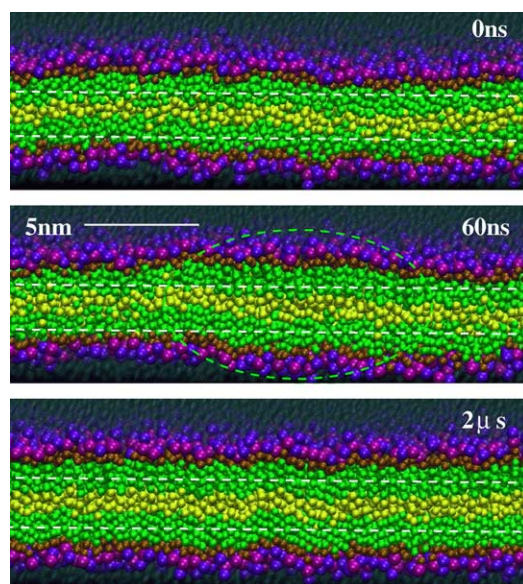


Fig. 2. Liquid-to-gel transformation in a bilayer consisting of 2048 DPPC lipids. The bilayer is cut to reveal the interior. The lipids are colored using the same color scheme as in Fig. 1, but with the terminal tail group depicted in a lighter shade of green. The bilayer is quenched from  $T = 325$  to 283 K, about 15 K below the main phase transition temperature of the coarse grained DPPC. Right after the quench, at  $t = 0$ , the bilayer is still in a disordered, fluid state. After 60 ns, almost half of the lipids have formed a gel domain (encircled) characterized by highly ordered tails and a concomitant increase in local bilayer thickness. Note the correlation in order of the lipid tails between the leaflets. Eventually, the whole bilayer patch is converted into a gel phase. The dashed lines indicate the approximate position of the C2 tail sites which are shown in Fig. 3. (For interpretation of the references to color in this figure legend, the reader is referred to the web version of the article.)

trix. These fluid domains appear stable for a relatively long time, eventually merging into one single domain (snapshot at 1  $\mu$ s). It takes another 1  $\mu$ s for this liquid domain to disappear. The total time required for the complete transformation from the liquid to gel phase is close to 2  $\mu$ s. Only small defects in the gel lattice persist on longer time scales. The area/lipid of the gel phase in the CG model is 0.465 nm<sup>2</sup>, close to the experimentally determined area/lipid of 0.46 nm<sup>2</sup> for DPPC (Nagle and Tristram-Nagle, 2000). The final snapshot in Fig. 2 reveals that the gel phase is untilted, rather than tilted as is observed experimentally. This issue will be addressed in more detail further on.

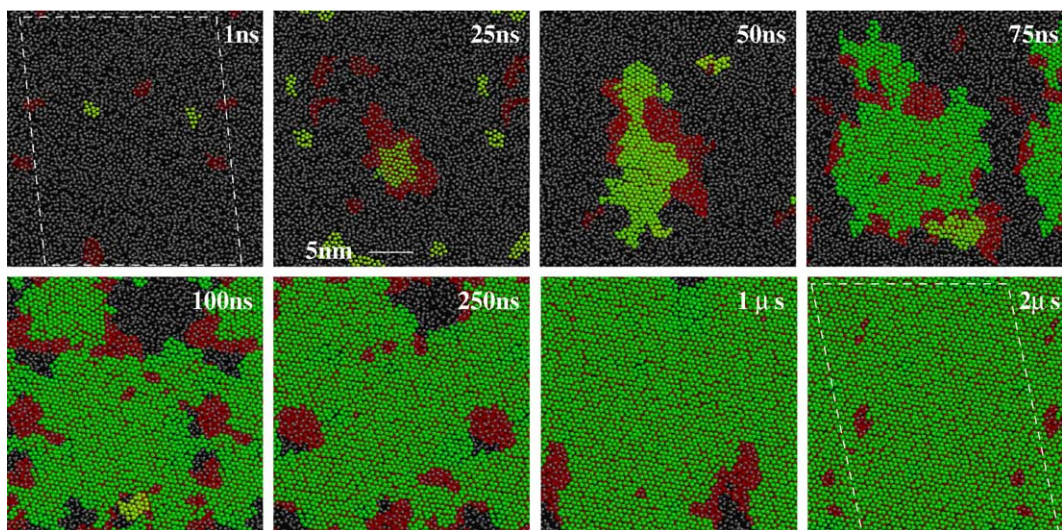


Fig. 3. Top view of the same liquid-to-gel transformation process as depicted in Fig. 2. Here, the bilayer is viewed from above, with only the two second tail (C2) sites being shown to highlight the formation of the gel phase (the first tail sites are the ones attached to the glycerol backbone). Tail sites that are in a fluid state are colored light grey, tails in the gel state are colored either green (upper monolayer) or dark red (lower monolayer). Small gel clusters are colored in a somewhat lighter shade compared to bigger clusters. The lateral box shape is indicated by dashed white lines in the first and last frame. Initially, only small, unstable gel domains are formed inside the fluid matrix. After 25 ns, a small gel domain has appeared that remains stable and grows rapidly, until at  $\sim 100$  ns the gel matrix has percolated in both lateral directions. A few fluid domains remain trapped and are seen to merge into one single domain which eventually ( $\approx 2 \mu\text{s}$ ) disappears, thereby completing the phase transformation. Only small defects in the gel lattice persist on longer time scales. (For interpretation of the references to color in this figure legend, the reader is referred to the web version of the article.)

### 3.1.2. Monolayer coupling

Next, we turn to the coupling between the two monolayers during the transformation process. Fig. 2 shows that a strong coupling exists between the ordering of each of the two monolayers. Initially, however, this is not the case. Before the critical cluster has formed, gel domains are seen to form independently in both monolayers (see first snapshot in Fig. 3). Formation of the critical cluster, i.e. the cluster that will grow, seems to require the gel phase to involve both monolayers simultaneously (second snapshot in Fig. 3). During the growth of the cluster, the coupling remains strong; whenever lipids are triggered to adopt an ordered state in one of the monolayers, the other monolayer follows quickly (on a time scale between 0 and 10 ns). The coupling persists also during the final stages of the transformation process. In the remaining fluid domains, both monolayers are fluid (last four snapshots in Fig. 3).

### 3.1.3. Characterization of intermediates

The graphical images presented above show a liquid to gel transformation upon cooling of a DPPC bilayer patch at  $T = 283$  K. Repeating the simulation starting from different starting structures reveal the same transformation pathway on a comparable time scale. The pathway is very similar irrespective of whether the system is quenched to a temperature just within the gel phase regime or by a larger amount. The kinetics of the transformation process, however, depend very strongly on the temperature. This is illustrated in Fig. 4, which shows examples of the time evolution of the number of lipids that are in the gel phase for systems quenched to different temperatures. All systems consisted of 2048 lipid molecules, starting from the same fluid state at  $T = 325$  K. The shape of the curves obtained at different temperatures are found to be very similar. Based on this similarity, we identify four distinct stages of the phase transformation process. During stage I, the bi-

layer is in a supercooled fluid state. Stage I is characterized by a low overall concentration of gel phase lipids, which remains essentially constant. Fast fluctuations can be seen (especially noticeable in Fig. 4 for the curve at  $T = 285$  K) which are due to small gel clusters forming and disappearing on a nanosecond time scale. These are so-called heterophase fluctuations. Do to their small size, the line tension dominates the thermodynamic driving force (Eq. (1)). Such domains therefore still have a higher free energy than the surrounding medium, and the probability of their formation will scale with the Boltzmann factor. Eventually, a gel domain forms that is large enough to overcome the critical energy barrier (Eq. (3)). This is the so-called critical nucleus. The size of the critical nucleus also depends on the thermodynamic driving force (Eq. (2)). A lower temperature increases the driving force, reducing the size of the critical nucleus. At  $T = 270$  K, the size of the critical nucleus is of the order of 10 lipids per monolayer, whereas at  $T = 285$  K the size is around 40 lipids per monolayer. The end of stage I, which we call the “nucleation” stage, is reached once the critical nucleus has formed (see the snapshot at  $t = 25$  ns in Fig. 3). The critical nucleus can lower its free energy by adding more gel lipids. This is observed in stage II, the “growth” stage, which is characterized by a rapid increase in the fraction of gel lipids. Initially, the growth rate of the cluster follows Eq. (6), with the radius of the cluster increasing in time linearly. Fits to Eq. (6) for each of the selected temperatures are included in Fig. 4. Gel lipids add to the growing cluster at a constant rate per unit length at the interface and the total amount of lipids that is added to the cluster (per unit time) increases as the interface becomes larger. The cluster growth rate follows Eq. (6) for some time, after which a cross-over to a limited growth regime is observed. The point where the growth rate can no longer be fitted to Eq. (6) is defined as the beginning of stage III, termed “limited growth”. The reason for the deviation from the ideal growth law is the interaction between the growing nucleus with either its own periodic image, or with other growing nuclei that have appeared independently. Multiple gel boundaries compete for the same fluid lipids, or merge thereby reducing the amount of gel boundary available to further lipid adsorption. The growth rate gradually decreases, until the percolation threshold of the gel phase is reached. As soon as the gel cluster percolates in two dimensions, the remaining fluid phase is trapped and further growth of

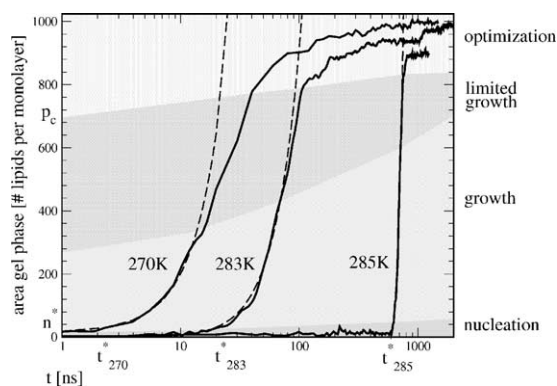


Fig. 4. Area of gel clusters as a function of simulation time for lipid bilayer patches consisting of 2048 lipids quenched to different temperatures below the main phase transition temperature. The different stages of the transformation process (nucleation, growth, limited growth, and optimization) are indicated schematically as shaded areas. On the ordinate axis  $t^*$  indicates the temperature dependent critical time required to nucleate a stable gel domain. At times  $t > t^*$ , the gel phase grows, initially fast as long as the gel domains do not interact. Dashed lines represent fits to the curve based on the theoretically predicted growth rate (Eq. (6)), distinguishing the fast growth stage from the limited growth stage. On the co-ordinate axis,  $p_c$  indicates the percolation threshold of the gel phase which marks the onset of the optimization stage. See text for details.

the gel clusters becomes much more difficult. The final stage of the transformation process, the “optimization” stage (stage IV), in which the remaining lipids in the fluid phase undergo the transition to a gel state. This requires the largest amount of time. The stability of the liquid domains can be attributed to the low compressibility of the gel matrix. The freezing of the trapped fluid domains is associated with a reduction in the local area per lipid. This requires a global reorganization of the gel matrix. Simulations performed on smaller size systems show that the fluid domains indeed disappear more rapidly; for the smallest systems studied (128 lipids), no metastable intermediate phase containing fluid domains was observed. Through diffusive motion, the fluid domains can merge into larger domains, minimizing the line tension between the gel and fluid phase. The merging can be seen in Fig. 4 (most clearly visible for the curves at  $T = 270$  and 283 K) as a step-wise increase of the number of gel phase lipids right after the fusion of two fluid domains. The phase transformation process is completed when the final remaining domain freezes.

The general pathway observed in our simulations can be summarized as a four-stage transformation process: first nucleation, followed by growth, limited growth, and finally optimization of the gel phase. Fig. 4 shows that the kinetics of the multiple stages are very much temperature dependent. Especially, the time required for nucleation is very temperature sensitive. This is a direct consequence of the height of the critical energy barrier for nucleation (Eq. (3)), which is exponentially related to the critical formation time (Eq. (4)). The height of this barrier is, approximatively, inversely proportional to the magnitude of the temperature quench (Eqs. (3) and (7)). Because of the exponential growth in the barrier crossing time, a simulation quenched to  $T = 290$  K never reaches the growth stage in a multi-microsecond simulation, although in the next section the actual transition temperature is shown to be in fact higher ( $T = 295$  K). At 270 K, the nucleation time is only a couple of nanoseconds. Consequently, the nucleation stage can hardly be distinguished from the growth stage. Some representative snapshots of the transformation process at 270 K are shown in Fig. 5. The first snapshot indicates the appearance of multiple stable clusters within a period of ten nanoseconds. Due to the high concentration of growing gel clusters, the stage of unhindered growth is relatively short. Clusters are seen to merge within 20 ns, forming already a percolative network after 40 ns. It is interesting to compare the structure of the percolating cluster at  $T = 270$  K to the structure obtained at  $T = 283$  K (Fig. 3, snapshot at 100 ns). At  $T = 270$  K, the percolating cluster is more irregular, containing more defects, compared to the structure at  $T = 283$  K which appears denser and more spherical. The irregular shape at lower temperature can be explained by two effects. First, the percolating cluster is an assembly of independently formed clusters, second, the time to optimize its structure has been relatively small. The difference is further illustrated by the snapshot taken from the simulation at  $T = 285$  K (Fig. 5), showing a single growing cluster of near spherical shape containing hardly any defects. The coupling between the two monolayers appears equally strong both at low and high temperatures.

#### 3.1.4. Connection to experiment

The temperature dependent kinetics as observed for the simulated systems does not tell the whole story. Combined X-ray diffraction and pressure-jump relax-

ation experiments (Erbes et al., 2000), for instance, show that the kinetics of the order–disorder transformation strongly depend on the cooling or heating rate. Under non-equilibrium conditions, intermediate structures may appear that cannot be detected close to equilibrium. Moreover, the macroscopic completion of the phase transition is often limited by the redistribution of water, a kinetic aspect that is absent in the simulations which are performed at constant hydration level. From the temperature dependent data of the cluster growth in the simulations, however, two important thermodynamic parameters can be derived that characterize the transformation process and which can be compared directly to results based on experimental measurements. These are the line tension  $\gamma$  and the entropy difference  $\Delta s$ . The line tension is a measure of the energy cost that arises from the packing frustration of a lipid in the gel phase bordering a lipid in the fluid phase. The entropy difference measures the entropy loss of a lipid in an ordered, gel state, with respect to a disordered, fluid state. According to Eqs. (2)–(4) and (7), both the critical cluster size and the logarithm of the critical time scale linearly with  $1/\Delta T$ , with slopes given by  $\gamma\sigma/\Delta s$  and  $\gamma^2\pi\sigma/\Delta skT$ , respectively (see Section 2). The scaling of the critical time and cluster size with the inverse of the change in temperature is shown in Fig. 6. The data points were obtained from simulations of gel formation in patches of 2048 lipids, quenched to temperatures ranging from 25 to 5 K below the estimated macroscopic transition temperature (295 K). Multiple simulations (typically in between three and five) using independent starting conditions were analyzed to improve the statistics. The simulations discussed in the preceding paragraph form part of the set used in this analysis. Fig. 6 shows the anticipated linear behavior observed for the critical time and cluster size. From a simultaneous fit of both curves, the following estimates for the line tension and the entropy difference were obtained:  $\gamma = 3 \pm 2$  pN and  $\Delta s = -0.05 \pm 0.03$  kJ mol<sup>-1</sup> K<sup>-1</sup>. Note that  $\Delta s$  is defined as the difference of entropy of a lipid in the gel with respect to the fluid phase. A negative value thus corresponds to a higher value of the entropy in the fluid phase, as expected. Due to the large spread in individual measurements, indicated by the error bars in Fig. 6, the estimates for the line tension and the entropy difference show a considerable range of uncertainty. It is tempting, however, to compare the simulation results to the experimental results reported

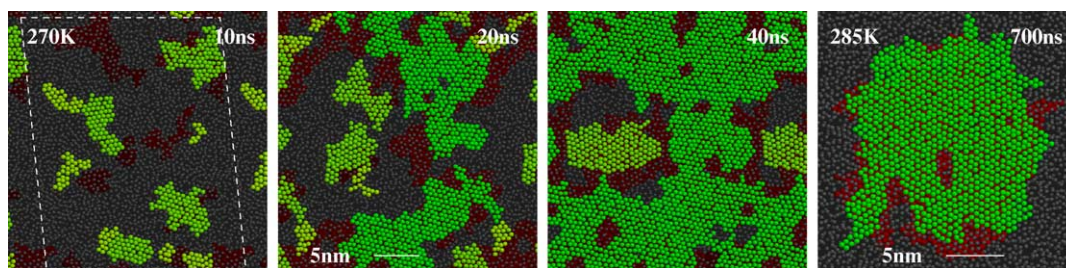


Fig. 5. Representative snapshots of the phase transformation process from the liquid to gel phase at lower ( $T = 270$  K, leftmost three) or higher temperature ( $T = 285$  K, rightmost) with respect to the gel formation shown in Fig. 3 ( $T = 283$  K). At  $T = 270$  K, 25 K below the phase transition temperature, cluster nucleation occurs much faster, with multiple clusters starting to grow simultaneously ( $t = 10$  ns). The growing clusters start merging ( $t = 20$  ns), forming a percolating cluster of highly irregular shape ( $t = 40$  ns). At  $T = 285$  K, only 10 K below the transition temperature, the nucleation process takes much longer. The snapshot shows the growing cluster at the end of the growth regime. The shape of the cluster is more regular compared to the shape of the clusters obtained at lower temperatures. Coloring and viewing direction as in Fig. 3. (For interpretation of the references to color in this figure legend, the reader is referred to the web version of the article.)

by Kharakoz and Shlyapnikova (2000). Using a combination of different experimental techniques (calorimetric, densitometric, and acoustic), these authors analyzed the behavior of small gel clusters appearing in DPPC vesicles at temperatures close to the main phase transition temperature. Within the framework of heterophase fluctuations (Frenkel, 1946; Kharakoz and Shlyapnikova, 2000), a kinetic model was derived from which the line tension and entropy difference could be obtained. The values reported are  $\gamma = 4$  pN and  $\Delta s = -0.14$  kJ mol<sup>-1</sup> K<sup>-1</sup>. As the experimental data were obtained from microscopically small clusters, the results should be directly comparable to the results obtained from the simulations. Within the error bars, the estimate of the line tension is identical for the simulated and the experimental system. The entropy difference, although of the same order of magnitude, appears significantly smaller in the simulation model. At least part of this difference can be explained as a direct consequence of the coarse graining nature of the underlying lipid model in the simulations. For real lipids, the entropy loss during the phase transformation is associated with ordering of each of the tail segments. As each CG site represents a group of four methylenes, the internal entropy within each of these groups is incorporated implicitly. During the phase transformation, this part of the total entropy remains constant in the CG model, leading to an underestimation of the entropy difference.

Apart from the scaling of the critical time and cluster size, the cluster growth rate is also shown in Fig. 6. The growth rate was obtained from fitting of the time-dependent cluster size (as shown in Fig. 4) to Eq.

(6). The growth rate represents the average speed at which the cluster radius expands during the fast growth stage, i.e. the stage where the clusters grow without feeling the presence of other clusters (or its periodic image). For small  $\Delta s \Delta T / kT$ , the cluster growth rate is expected to increase linearly with the temperature interval, following  $u \simeq -u_{\max} \Delta s \Delta T / kT$  (combining Eqs. (5) and (7)). A linear fit to the data points, using  $\Delta s = -0.05$  kJ mol<sup>-1</sup> K<sup>-1</sup> as derived previously, results in an estimate for the maximum growth rate  $u_{\max} = 0.35 \pm 0.2$  nm ns<sup>-1</sup>. According to the kinetic model of Kharakoz and Shlyapnikova (2000), the maximum growth rate is reached when the lipids add irreversibly to the growing gel cluster. The apparent overshooting of the maximum growth rate at the lowest temperatures studied in our simulations ( $\Delta T > 20$  K) points to a different mechanism of growth in supercooled bilayers. A likely explanation is that, instead of individual lipids, small clusters that nucleate in the vicinity of the growing gel cluster are adsorbed. For instance, in Fig. 5, the snapshot at  $t = 20$  ns for the system quenched to  $T = 270$  K, 25 K below the transition temperature, shows multiple small clusters close to the growing, larger cluster(s). The estimate of  $u_{\max} = 0.35$  nm ns<sup>-1</sup> is about an order of magnitude larger than the value reported by Kharakoz and Shlyapnikova (2000). Under the assumption that the maximum growth rate is limited by the time scale of the rotational reorientation of the fluid lipids at the gel–fluid boundary, the overestimation of the growth rate in the CG model could be caused by relatively fast rotational dynamics. The dynamics of the lipids will be discussed later.

### 3.2. Gel–liquid transformation

#### 3.2.1. Transformation process

Fig. 7 shows an example of the stages observed in the reversed process, i.e. the melting of the ordered gel phase to a disordered fluid phase. The process of melting appears to follow the same stages as observed during freezing, but in reverse order. Fig. 7 may be compared to Figs. 3 and 5, time reversed, to see the similarity of the transformation process. When heated to 310 K, the gel phase remains metastable for about 5 ns. Seeded by defects present in the gel lattice, small fluid patches start to appear as a consequence of the clustering of these defects. The relationship between these defects and the hexatic phase is discussed below in more detail. The fluid domains immediately start growing (snapshot at 10 ns), condensing into larger fluid patches (Fig. 7, snapshots at 15 and 20 ns). After ~25 ns, the fluid phase has percolated, leaving essentially one large gel patch surrounded by the fluid phase. The gel patch melts further over the next 10 ns, until the fluid phase is recovered at  $t = 40$  ns. Depending on the gap between the temperature at which the system was simulated and the actual transition temperature, the fluid domains can appear metastable on much longer time scales (microseconds at  $T = 300$  K), similar to the “optimization” stage of the freezing transformation. At even lower temperatures,  $T = 290$  K, the gel phase is not observed to melt on the microsecond time scale of the simulation. As was discussed in the previous section, at this temperature a fluid patch remains fluid. The hysteresis that we observe in the simulations of the main phase transformation is quantified further in Section 3.3.1.

#### 3.2.2. Hexatic phase

In this section we discuss the hypothesis that the lipid gel phase might be of hexatic nature, or more generally, that two-dimensional melting is a two-stage process governed by the unbinding of dislocations. According to the theoretical predictions of Kosterlitz, Thouless, Halperin, Nelson, and Young (KTHNY) (Kosterlitz and Thouless, 1973; Halperin and Nelson, 1978) melting in two dimensions occurs in two steps. In the solid phase, the only lattice defects that can be supported at finite temperature are so-called disclination quadrupoles, consisting of pairs of tightly bound dislocations. Disclinations are any lattice sites having other

than six neighbors, and dislocations consist of a bound pair of a five- and seven-fold disclination. During the first melting step, the disclination quadrupoles unbind resulting in free dislocations. Free dislocations can be interpreted as an extra lattice row inserted, and have the effect of destroying the long-range translational order while preserving a quasi-long-range orientational order. The second step consists of subsequent unbinding of these dislocations into free disclinations, which would destroy any remaining long-range order leading to a fluid phase. The intermediate phase is called hexatic. In a strict sense it is limited to a phase with free dislocations, but in general it is applied to phases which show long-range orientational order and short-range translational order. Melting along grain boundaries, an alternative theory proposed by Chui (1983), involves the formation of strings of dislocations rather than their unbinding. To explore the nature of lattice defects present in the CG DPPC gel phase, we performed a Voronoi analysis (see Section 2). Based on the Voronoi analysis, the number of neighbors for each of the lipid tails was calculated. The results of this analysis are shown in Fig. 8 for gel patches at temperatures in the vicinity of the estimated macroscopic phase transition temperature ( $T = 295$  K). In order to study the long-range order, the system size was extended to measure  $50 \text{ nm} \times 50 \text{ nm}$ , consisting of 8192 lipids. The simulations were started from a perfectly ordered (i.e. defect-free) gel phase.

At 295 K, the lattice remains almost perfectly hexagonal, with only a few defects present. Defects only occur as tightly bound pairs of dislocations (disclination quadrupoles), which preserve the long-range order. As the temperature is increased to 300 K, more defects are seen to appear in the lattice. In the course of time, however, these defects tend to aggregate into higher order clusters of disclinations. Eventually, a clear phase separation can be seen between a small area of high disclination density surrounded by an area of low disclination density. The area of high disclination density is in fact a region of fluid DPPC, corresponding to the metastable intermediate stage of the phase transformation as depicted in Fig. 3 (snapshots at 250 ns or 1  $\mu\text{s}$ ) or 7 (snapshots at 15 or 20 ns). Unbinding of disclination quadrupoles into dislocations, and subsequent unbinding of dislocations into free disclinations, as predicted by KTHNY (Kosterlitz and Thouless, 1973; Halperin and Nelson, 1978), is not observed. Free dis-

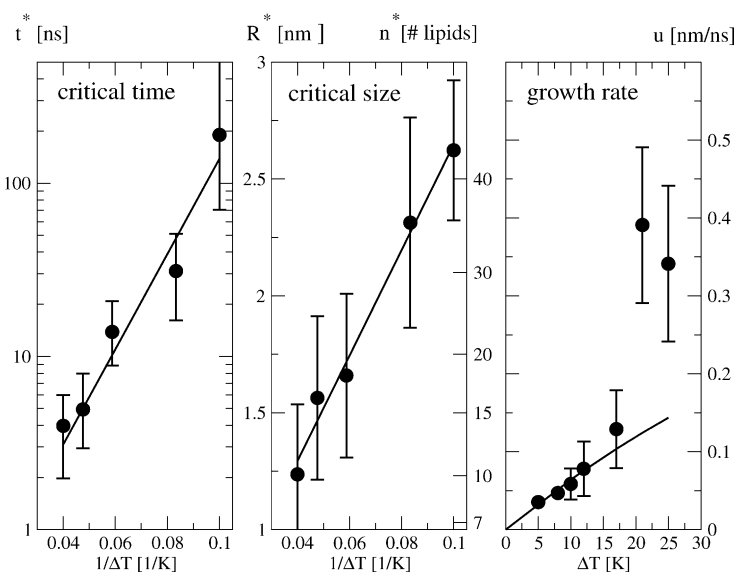


Fig. 6. Temperature dependent scaling of cluster growth. The left panel shows the scaling of the critical nucleation time  $t^*$  with inverse temperature difference  $1/\Delta T$ , the middle panel shows the scaling of the critical radius  $R^*$  (left axis) or size  $n^*$  (right axis) with  $1/\Delta T$ , and the right panel shows the cluster growth rate  $u$  vs.  $\Delta T$ . The data points were obtained from simulations of gel formation in patches of 2048 lipids, quenched to temperatures ranging from 25 K to 5 K below the estimated macroscopic transition temperature (295 K). The error bars indicate the spread of values obtained from multiple independent simulations. The solid lines are linear fits to the data points. See text for details.

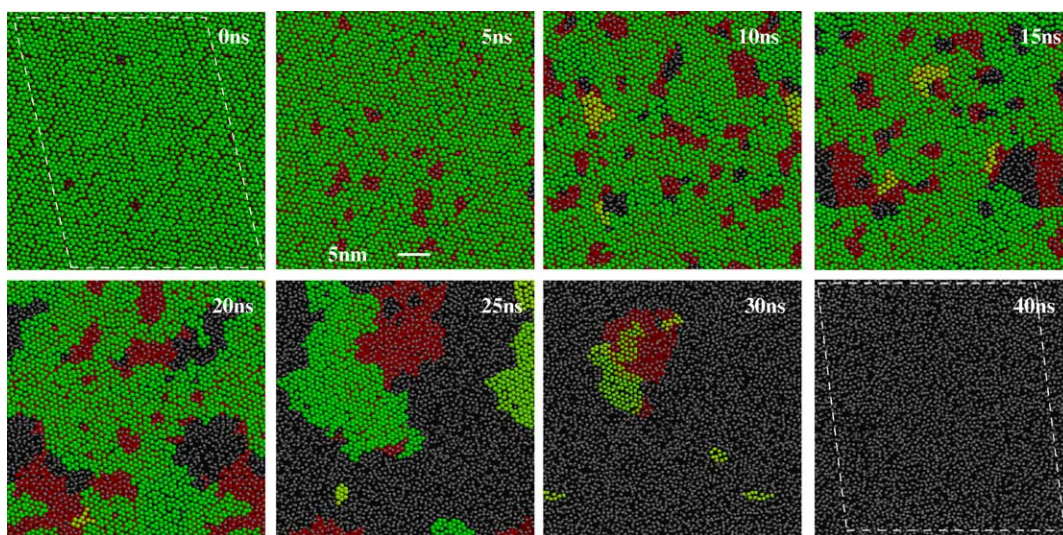


Fig. 7. Gel-to-liquid transformation in a DPPC bilayer. A gel phase DPPC bilayer composed of 2048 lipids was heated to  $T = 310$  K, about 15 K above the main phase transition temperature of the coarse grained DPPC. Same viewing and color coding as in Fig. 3. At 310 K, the gel phase appears metastable for about 5 ns, although many small defects are visible. The defects subsequently concentrate, forming small patches of the fluid phase inside the gel matrix within 10 ns. These patches rapidly grow, and merge into large fluid domains, until after  $\sim 25$  ns the fluid phase has percolated, leaving a large gel domain. This gel domain requires another 10 ns to fully melt, thereby completing the gel to fluid transformation. (For interpretation of the references to color in this figure legend, the reader is referred to the web version of the article.)

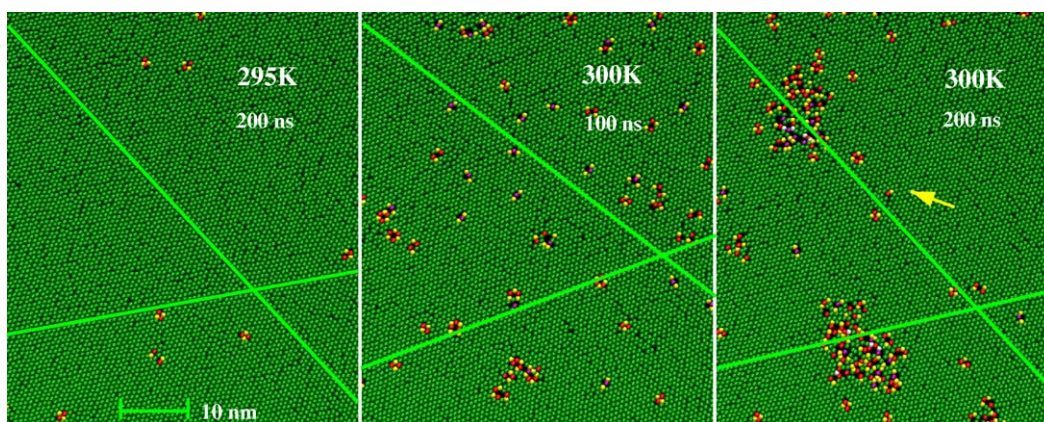


Fig. 8. Voronoi analysis of a bilayer consisting of 8192 lipids simulated at different temperatures close to the phase boundary. Based on the Voronoi analysis of the positions of the C2 tails atoms, the number of neighbors is calculated. Normal hexagonal ordering, i.e. six neighbors, is indicated as green. The other color codes indicate four-fold (white), five-fold (yellow), seven-fold (red), and eight-fold (purple) disclinations. The green lines illustrate the long-range translational order present in each of the systems. The arrow points at an isolated dislocation. (For interpretation of the references to color in this figure legend, the reader is referred to the web version of the article.)

locations do form occasionally (see arrow in Fig. 8), but appear only at very small concentrations. Formation of grain boundaries, as predicted by Chui (1983), is not observed either. The melting process observed in the simulations appears to proceed via the concentration of defects into small regions, which adopt a fluid like character. When the density of fluid regions exceeds some critical threshold, the transformation to the fluid phase is triggered. Throughout the melting process, long-range translational order still persists as is shown in Fig. 8. Experimental evidence has been presented by Smith et al. (1990), characterizing the lateral correlation in the gel phase of DMPC (myristoyl tails) as relatively short-ranged ( $\sim 20$  nm), suggesting a hexatic phase. The interpretation of this observation remains unclear. One could argue that the periodicity of the systems simulated prevents the formation of independently oriented subdomains, requiring system sizes exceeding the correlation length by at least an order of magnitude. Hexatic type ordering is seen in our simulations, but only as an intermediate stage. Fig. 5 shows that independently formed gel domains which start interacting and fusing can form an intermediate structure in which orientational correlation is enforced but translational order limited. Rearrangement of these separate gel domains into a fully ordered gel lattice is, however, observed on the nanosecond time scale. It is possible that on macroscopic length scales and at temperatures

close to the phase boundary such an intermediate stage might be long lived, giving rise to an apparent hexatic lipid gel phase. The experimental measurements of Sun et al. (1994) on gel DPPC indicate long-range translational order exceeding 290 nm. Our results point to translational order over length scales of at least 50 nm, in agreement with these measurements.

### 3.3. Transition temperature

#### 3.3.1. Effect of hysteresis

It was shown in the preceding sections that melting and freezing of the bilayer follow similar stages, but do not occur at the same temperature. A considerable amount of hysteresis is observed. Experimentally, the formation of ordered lipid phases is also subject to strong hysteresis. Gel phases can be observed to remain stable well beyond the transition temperature, and the liquid phase can be supercooled. The major reason for hysteresis is kinetic trapping. Furthermore, local overheating or undercooling may give rise to so-called van der Waals loops, if the system is unable to conduct the heat required (melting) or produced (freezing) fast enough (Esselink et al., 1994). If the rates of cooling or heating are slow enough (quasi-static), the hysteresis will narrow. To study the effect of time scale on the hysteresis in our simulations, both heating and cooling runs of lipid bilayers were performed over a range of tem-

peratures and the time required to observe the onset of the phase transformation measured. Note that, instead of a quasi-static cooling, the simulated bilayers experience a sudden temperature drop. The right side of Fig. 9 shows the apparent transformation time as a function of the temperature. As expected, the observed hysteresis between the transformation temperature from gel to liquid and the transformation temperature from liquid to gel becomes smaller as the time window increases. In other words, the transformation temperatures converge to the ‘real’ transition temperature which would only be observed on macroscopic time scales. Extrapolation of the results indicate a macroscopic transition temperature of around 300 K. However, a true macroscopic system also exceeds the length scale of the simulated systems by many order of magnitudes. The effect of system size on the transformation temperatures is shown in the left panel of Fig. 9. Increasing the system size has the same qualitative effect on the hysteresis as increasing the time scale, i.e. narrowing it. The effects of time and length scales are in fact strongly related. As we have shown in the preceding section, the transformation is triggered by a critical fluctuation which becomes more likely if longer time scales or larger samples are considered. The variation in length scale has another, secondary effect. Decreasing the size of the system suppresses undulations and enforces the spatial correlations through the periodic replicas of the simulation box. Both these effects tend to stabilize the gel phase. For the cooling simulations, this effect diminishes the likelihood of forming a gel domain of critical size, giving rise to a lower system size dependency of the phase transformation temperature. For the heating simulations, on the other hand, the effects combine to a more pronounced system size dependency. Extrapolation of the system size towards infinity suggests a macroscopic transition temperature in the range 290–300 K. To further pinpoint the transition temperature, the system depicted in Fig. 3 at  $t = 75$  ns (i.e. half gel half liquid) was taken as a starting configuration and simulated at 290, 295, and 300 K. At 290 K, the gel domain keeps on expanding, whereas at 300 K it melts. At 295 K, the gel domain appears stable during a 1  $\mu$ s simulations, indicating close vicinity to the phase boundary. The estimated transition temperature of the coarse grained DPPC is  $T = 295 \pm 5$  K.

Experimentally (Koynova and Caffrey, 1998; Nagle and Tristram-Nagle, 2000), DPPC forms a rippled gel

phase ( $P_{\beta'}$ ) at the main phase transition temperature  $T_{\text{main}} = 315$  K. The ripple phase is stable over a narrow temperature range only, and converts to a tilted gel phase ( $L_{\beta'}$ ) at the so-called pre-transition temperature at  $T_{\text{pre}} = 307$  K. Although tilt cannot be reproduced by the standard CG model (the simulated phase transition is  $L_{\alpha}$  to  $L_{\beta}$ ), the phase transition temperature of the CG model compares favorably to the experimental transition temperature. Depending on which of the two transition temperatures to compare to, the temperature difference between the fluid-to-gel transition in the CG model versus real DPPC is 10–20 K. Note, the CG model is unable, by its very nature, to distinguish between lipids that differ in tail length by only one or two methylene units. The same CG set-up as depicted in Fig. 1 would be used to model DMPC. The experimental transition temperatures for DMPC are about 20 K lower than DPPC (Koynova and Caffrey, 1998), putting the CG model somewhere in between of DMPC and DPPC.

### 3.3.2. Effect of hydration

Apart from differences in system size and time scale, there is another important difference between the experimentally observed order/disorder transformation in lipid bilayers and the one simulated. Under experimental conditions, the hydration level decreases during the transformation from the fluid to ordered state. In the simulations, the size of the system is too small for the water to be able to phase separate and therefore the hydration level remains constant (at 32 water molecules/lipid). In order to test the effect of the hydration level on the observed phase transformation temperatures, a series of simulations of small samples (128 lipids) was performed, subsequent samples containing less water molecules. The results are depicted in Fig. 10. Within the statistical accuracy, the transformation temperature remains constant over the hydration range 15–48 water molecules/lipid, largely covering the difference between the experimental swelling limits of the gel and the fluid phase. The neglect of dehydration during the simulated phase transformation is therefore not expected to be very important. At hydration levels below the swelling limit of the gel phase, a strong increase in the phase transformation temperature is observed, however. This behavior is in agreement with the experimentally observed dependence of the transition temperature on the level of hydration (Koynova and

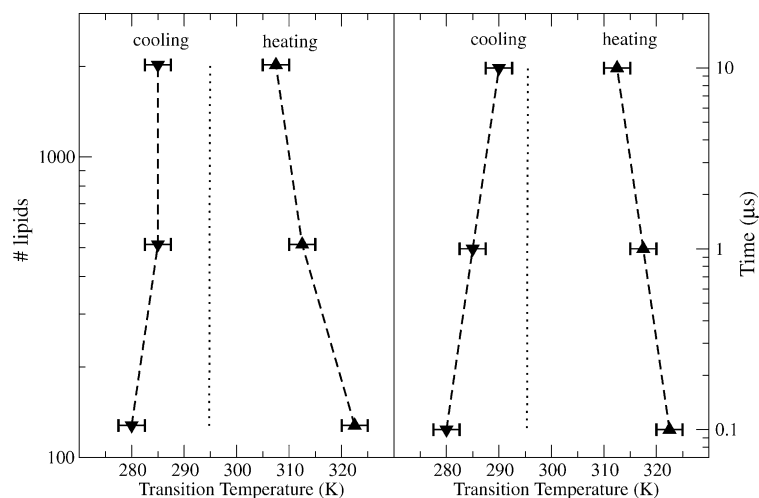


Fig. 9. Gel–liquid transformation temperature of DPPC bilayers as a function of system size (left) and simulation time (right). Data points labeled as ‘cooling’ and ‘heating’ indicate the temperature to which the bilayer needs to be cooled (starting from the fluid phase) or heated (starting from the gel phase) before a spontaneous phase transformation is observed. Between the cooling and heating lines, the bilayer can exist either as a metastable gel or supercooled fluid. The data displayed in the left panel were obtained from 100 ns simulations, the data displayed in the right panel on systems consisting of 128 lipids. The dotted lines denote the estimate of the macroscopic phase transition temperature for a coarse grained DPPC bilayer,  $T = 295$  K.

Caffrey, 1998). For almost dehydrated samples, chain melting takes place at 342 K (Hentschel et al., 1989), an increase of close to 25 K. The simulations show an increase between 15 and 20 K. The reason for the increase in the phase transition temperature is likely to be the suppression of both small scale protrusions and larger scale undulatory modes.

### 3.3.3. Effect of curvature

Related to the effect of undulations is the effect of curvature. Both increased undulations and increased curvature will tend to stabilize the fluid phase over the gel phase. In order to study the effect of curvature on the phase transformation process, a small vesicle (diameter 20 nm) consisting of more than 2500 DPPC lipids was cooled to a temperature of 283 K, well below the estimated phase transition temperature of  $T = 295$  K. During the time course of the simulation (0.5  $\mu$ s), no gel formation was observed. Note that a lamellar system of similar size and at the same temperature starts forming gel patches within tens of nanoseconds, and almost completely freezes within 1  $\mu$ s (see Fig. 3). Further reduction in the temperature to 270 K did not induce the formation of a gel phase. Only at 265 K, patches of gel could be seen to develop, a process stopped by the

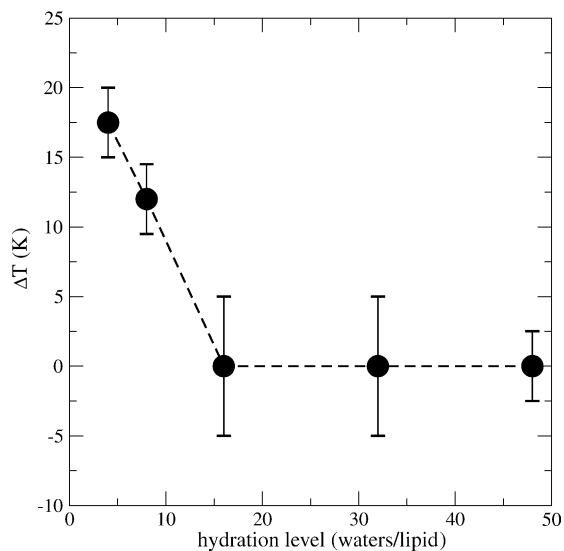


Fig. 10. Shift in transformation temperature as a function of the hydration level. The transformation temperature was obtained from simulations of small samples (128 lipids). The error bars indicate the amount of hysteresis observed. The transition temperature is estimated as the midpoint.

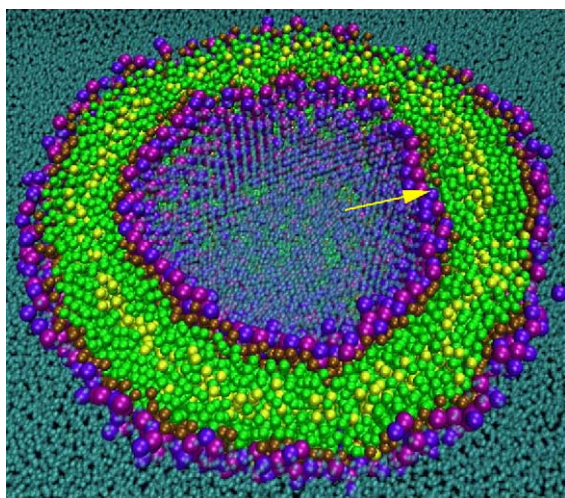


Fig. 11. Snapshot of a small vesicle ( $\sim 20$  nm diameter) cooled to 265 K. Only half of the vesicle is shown to reveal its interior. Whereas lamellar DPPC rapidly (within 10 ns) adopts a gel phase at 265 K, the vesicle remains fluid on a time scale of hundreds of nanoseconds. The strong curvature apparently suppresses global gel formation although small patches of ordered lipids do form locally (arrow). The snapshot shows the structure after 400 ns of simulation, the moment that the interior water freezes.

freezing of the interior water. A snapshot of the vesicle at the end of the simulation is shown in Fig. 11. Ordered domains, characterized by a larger membrane thickness and strong alignment of the terminal methyl groups, can be seen clearly. Freezing of the interior water, but not of the exterior water, can be explained by the Laplacian overpressure inside the vesicle. Experimentally, depression of the phase transition temperature is also observed for strongly curved vesicles. For vesicles smaller than  $\sim 70$  nm in diameter the phase transition temperature gradually decreases with decreasing vesicle size (Biltonen and Lichtenberg, 1993; Koynova and Caffrey, 1998). For vesicles with a diameter of  $\sim 35$  nm, the transition temperature decreases by  $\sim 5$  K. Vesicles as small as the one simulated here (diameter 20 nm) cannot be formed experimentally. It is reasonable, however, that the effect of curvature on the transition temperature will be even larger in the vesicle simulated.

### 3.4. Nature of the ordered phase

#### 3.4.1. Lateral diffusion

To assess the nature of the ordered phase, first the lipid lateral and reorientational dynamics were eval-

uated. Apart from subtleties in lateral packing, for which it is doubtful that they can be reproduced by a coarse grained model, the major distinction between a gel and a crystal phase is in the nature of the lipid dynamics. Whereas the lipids are essentially frozen in a crystalline phase, the gel phase is characterized by fast rates of lipid lateral diffusion, which are only one or two orders of magnitude lower than those of the liquid-crystalline phase. The lipid lateral diffusion rate can be calculated from an MD trajectory from the slope at long times of the mean squared displacement (MSD). Fig. 12 shows the MSD curves for the center-of-mass of the lipids, averaged over  $5 \mu\text{s}$  of simulation and 512 lipids. Both in the fluid and in the gel phase, the MSD curves scale linearly with time, indicative of true Brownian diffusive motion. The distances covered by the lipids in the fluid phase are almost two orders of magnitude higher than those in the gel phase. At a temperature close to the macroscopic phase transition temperature ( $T = 295$  K), the nearest neighbor distance, around 0.7 nm, is covered in 10 ns in the fluid phase, whereas it requires close to  $1 \mu\text{s}$  in the gel phase. During a typical simulation run of  $5 \mu\text{s}$ , an area of  $250 \text{ nm}^2$  would be covered on average by the lipids in the fluid phase, while only  $2.5 \text{ nm}^2$  in the gel phase. Thus, whereas the lipids in the fluid phase are able to sample the entire box area during a simulation (the box area of a bilayer patch of 512 lipids would be around  $300 \text{ nm}^2$ ), in the gel phase movements are limited to a few nearest neighboring distances. It appears that the rate of diffusion in the gel phase is very sensitive to the number of lattice defects present. MSD curves obtained using systems containing various numbers of such defects show lateral mobilities up to five-fold larger than the ones shown in Fig. 12. The results plotted in Fig. 12 were obtained using an ideal defect-free gel bilayer, and therefore serve as an estimate of the lower bound of the lateral diffusion rates at the different temperatures.

The diffusion coefficients obtained from the slope of the MSD curves are plotted in the insert of Fig. 12 as a function of inverse temperature. In the fluid phase, the diffusion coefficients are in the range  $1\text{--}4 \times 10^{-7} \text{ cm}^2 \text{ s}^{-1}$  for the temperature range  $T = 285\text{--}350$  K (where the lowest temperatures apply to the supercooled fluid state). Experimentally, reported values for DPPC are  $0.6\text{--}2 \times 10^{-7} \text{ cm}^2 \text{ s}^{-1}$  between  $T = 315$

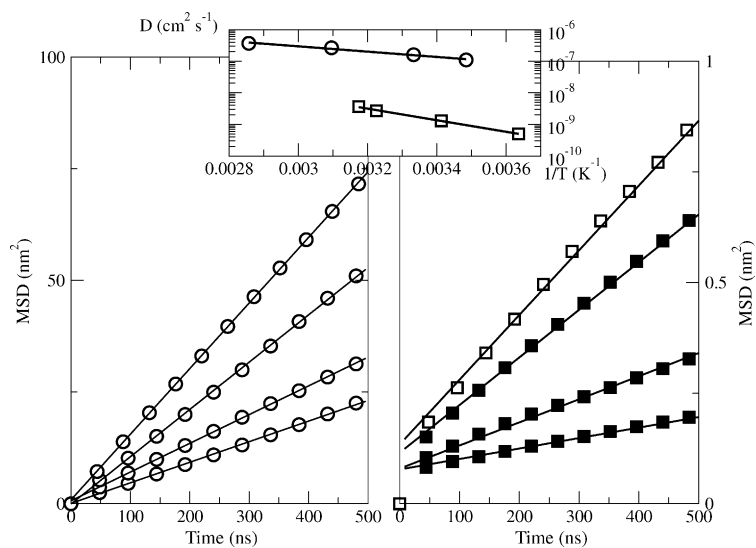


Fig. 12. Mean squared displacement of DPPC lipids at different temperatures in the fluid (left) and gel (right) phase as a function of time. Note the difference in the co-ordinate scale between fluid and gel phase. The solid lines are linear fits to the data points, from which the diffusion constant is obtained. The MSD curves apply to different temperatures. From top to bottom: 350, 325, 300, and 287 K for the fluid phase, and 315, 310, 293, and 275 K for the gel phase. The insert shows the diffusion constant on a logarithmic scale as a function of the inverse temperature. Assuming Arrhenius type behavior, the solid lines are linear fits corresponding to an activation energy of 16 kJ mol<sup>-1</sup> in the fluid and 35 kJ mol<sup>-1</sup> in the gel phase.

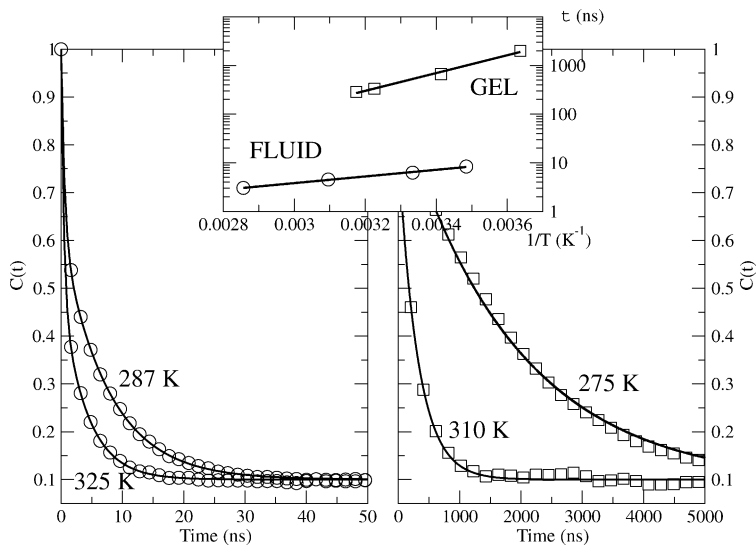


Fig. 13. Rotational autocorrelation function of the glycerol backbone vector in the fluid (left) and gel (right) phase. Note the difference in the ordinate scale between fluid and gel phase. The solid lines are double exponential fits to the data points. The inset shows the longer decay time on a logarithmic scale as a function of inverse temperature, where the solid line denotes a linear fit corresponding to an activation energy of 13 kJ mol<sup>-1</sup> in the fluid and 35 kJ mol<sup>-1</sup> in the gel phase.

and 335 K (pulsed NMR; Kuo and Wade, 1979) and  $1 \times 10^{-7} \text{ cm}^2 \text{ s}^{-1}$  at  $T = 321 \text{ K}$  (spin-label technique; Sheats and McConnell, 1978), although lower values are also reported ( $\sim 10^{-8} \text{ cm}^2 \text{ s}^{-1}$  at 325 K by NMR; Lee et al., 1995). More recent measurements on DMPC samples give  $1 \times 10^{-7} \text{ cm}^2 \text{ s}^{-1}$  at  $T = 300 \text{ K}$  (pulsed NMR; Orädd et al., 2002) and on POPC (palmitoyl-oleoyl-PC) samples  $2 \times 10^{-7} \text{ cm}^2 \text{ s}^{-1}$  at  $T = 322 \text{ K}$  (pulsed NMR of multilamellar liposomes; Gaede and Gawrisch, 2003). The range of diffusion rates obtained from the simulations appears to overlap with most of the experimental measurements. From the temperature dependence of the diffusion rate, the Arrhenius activation energy for lipid lateral diffusion can be determined. In the fluid phase, the activation energy is found to be  $16 \pm 2 \text{ kJ mol}^{-1}$ . This appears significantly lower compared to most recent experimental estimates which range from  $28 \text{ kJ mol}^{-1}$  (Filippov et al., 2003) and  $31 \text{ kJ mol}^{-1}$  (Gaede and Gawrisch, 2003) for POPC to  $49 \text{ kJ mol}^{-1}$  (Orädd et al., 2002) for DMPC. A value as low as  $15 \text{ kJ mol}^{-1}$  for DPPC has also been reported (Lee et al., 1995), however, making the interpretation of the experimental numbers difficult. In the gel phase, the range of diffusion rates obtained from the simulations is  $0.5\text{--}4 \times 10^{-9} \text{ cm}^2 \text{ s}^{-1}$  over a temperature range 275–315 K (where the highest values apply to a metastable gel phase). Experimentally, individual measurements are scattered widely, with values reported in the range  $0.04\text{--}16 \times 10^{-9} \text{ cm}^2 \text{ s}^{-1}$  at temperatures around 300 K (see Lee et al., 1995, for an overview). A drop of about two orders of magnitude in the lateral diffusion rates going from the liquid to the gel phase, as is observed in the simulations, seems reasonable. Again we note that the values obtained for the diffusion constants in the gel phase are very sensitive to the number of defects. If such defects also exist in macroscopic systems, they may explain some of the scatter observed in the experimental measurements. The activation energy for lipid lateral diffusion in the simulated gel phase is  $35 \pm 5 \text{ kJ mol}^{-1}$ , about twice as large as in the fluid phase. The higher activation energy reflects the much higher energy cost to create the necessary voids in the gel matrix with respect to the fluid matrix. Doubling of the activation energy across the main phase transition is in qualitative agreement with experimental measurements (Lee et al., 1995).

### 3.4.2. Rotational motion

Next, we turn to the rotational correlation times. Fig. 13 shows the decay of the rotational autocorrelation function (ACF) for the glycerol backbone vector (i.e. the vector connecting the two glycerol sites; see Fig. 1). The same systems were used as for the computation of the lateral diffusion coefficient. The rotational ACFs can be fitted to a double exponential, with a short correlation time describing the restricted rotational motion within the cage formed by the neighboring lipids, and a long correlation time required for full relaxation of the glycerol backbone vector.

The non-zero residual value originates from a preferred orientation of the glycerol backbone with respect to the bilayer normal, with the *sn* – 1 chain (in the CG model: the chain attached to the glycerol bead not attached to the headgroup) buried slightly deeper into the membrane. The short correlation time is of the order of  $500 \pm 200 \text{ ps}$ , not very temperature dependent, and similar in both the fluid and the gel phase. The difference of the long time rotational behavior in the gel vs. the liquid-crystalline phase, however, is large. Whereas the ACFs in the fluid phase decay rapidly (tens of ns) to their long time residual value, in the gel phase correlation times extend to the microsecond time scale. The long time correlation times obtained from the double exponential fits are plotted in the inset of Fig. 13. From the temperature dependence of the long time correlation, the predicted activation energies obtained from a linear fit are  $13 \pm 1 \text{ kJ mol}^{-1}$  in the fluid, and  $35 \pm 3 \text{ kJ mol}^{-1}$  in the gel phase. Thus, it appears that for the CG model the activation energies for rotational and diffusional motion are similar. Note, the rotational correlation time of the lipid headgroups is short (nanoseconds), both in the fluid and the gel phase (data not shown). Fig. 2 also shows that whereas the lipid tails become highly ordered in the gel phase, the lipid headgroups remain disordered. This is in agreement with the picture that arises from X-ray scattering measurements (Sun et al., 1994) and from simulations of gel formation in DPPC bilayers using an atomic model (de Vries et al., in press).

The main conclusion from the evaluation of the lateral and rotational dynamics of the ordered DPPC phase is that it is clearly a gel, and not a crystal phase. It is important to note that, although the dynamics in the gel phase are sensitive to the presence of defects, our results show that even in a perfectly ordered lattice the

lipids still possess diffusional and rotational freedom. Additional simulations in which the gel patches were cooled to temperatures below 270 K resulted in freezing of the water layer. It therefore remains unclear if a transformation to a true crystal phase can be observed with the CG model.

### 3.4.3. Tilt

A clear discrepancy with the available experimental results is the absence of tilt of the lipid tails with respect to the bilayer normal (see Fig. 2). DPPC, as well as DMPC and few other lipids are well known to form the tilted  $L_{\beta}'$  phase rather than the untilted  $L_{\beta}$  phase which is formed by PEs (phosphatidylethanolamines) for instance. The rationale for the formation of a tilted gel phase rather than an untilted one is the imbalance between the headgroup size and the optimal packing distance of the lipid tails. PCs have a relatively bulky headgroup and are unable to pack at the area preferred by the lipid tails. Consequently, the tails collectively tilt to optimize the interchain interactions. Experimentally, the tilt for DPPC is around  $30^\circ$  depending on the hydration conditions (Katsaras et al., 1992; Sun et al., 1994). In principle, tilt can be reproduced by CG models, as was shown by Kranenburg et al. (2003) and Stevens (2004). The reason for the inability of the current CG model to form a tilted gel phase originates from the fixed size of the tail sites, which were modeled to reproduce correct densities in liquid alkane phases (Marrink et al., 2004). Some of the entropic disorder present in an atomistic chain is therefore captured by the volume of the tail sites. Lowering the temperature cannot remove this volume, and therefore prevents the tilting of the chains. In order to study tilted gel phases, the volume of the tail sites should be reduced. Fig. 14 shows an example of the formation of a tilted gel phase for DPPC which is obtained using a slightly different force field in which the size of the tail beads is decreased by 10%. Now the tails prefer to pack at a somewhat smaller area, which can only be achieved through collective tilting. The tilt angle is close to  $30^\circ$ . In fact, a tilted gel could only be obtained at very low hydration. At higher hydration levels, the system spontaneously buckles, forming a ripple-like phase. This corresponds to the experimental situation for DPPC, which exhibits a ripple phase at temperatures and hydration levels intermediate of the liquid-crystalline and the gel phase. The structure of the ripple phase is likely linked to the

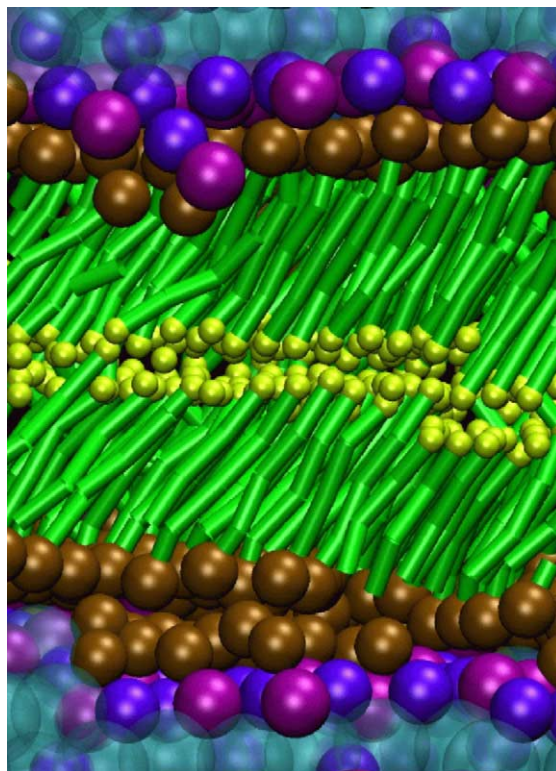


Fig. 14. Snapshot of a tilted gel phase ( $L_{\beta}'$ ) at low hydration. Reduction of the size of the tail beads by 10% induces tilting of the tails over an angle of  $30^\circ$  with respect to the bilayer normal. The same color scheme is used as in Figs. 1 and 2. (For interpretation of the references to color in this figure legend, the reader is referred to the web version of the article.)

tilting of the lipids (it is not observed for lipids which form untilted gel phases). The structure of tilted gel phases and the connection to the ripple phase has recently been studied by MD simulations in atomistic detail (de Vries et al., in press).

## 4. Conclusion

We have shown that a coarse grained model for DPPC can be used to simulate the main phase transformation of a lipid bilayer. The cooling of bilayer patches below the transition temperature triggers the formation of small gel domains, typically consisting of 20–80 lipids in both leaflets simultaneously. The time scale required for the formation of the initial cluster of ordered lipids depends strongly on both the system size and

the temperature. Once formed, these domains rapidly grow converting the fluid phase into a gel phase. A strong coupling is observed between the two monolayers. Small remaining fluid domains appear metastable up to microseconds. The transformation process can be summarized as a four-stage process: nucleation, growth, limited growth, and optimization. The reverse process, the melting of the gel into a fluid bilayer, follows the reverse pathway. A considerable hysteresis is observed in the transformation temperature, which is reduced upon system enlargement or upon increasing the time scale of the simulation. Extrapolation to a macroscopic bilayer suggests a transition temperature of  $295 \pm 5$  K, in between the experimental main phase transition temperature of DPPC and DMPC. Simulations of dehydrated samples and of a vesicular system show that both undulations and curvature stabilize the fluid phase.

The nature of the ordered low temperature phase is clearly a gel, and not crystalline. Lipid lateral diffusion rates are of the order of  $1 \times 10^{-9} \text{ cm}^2 \text{ s}^{-1}$ , a drop of about two orders of magnitude with respect to the fluid phase, in agreement with experimental measurements. The lipid headgroups remain disordered and fluid-like. No evidence is found for the existence of hexatic order in the gel phase. Unbound dislocations disrupting the long-range translational order cannot be supported by the gel matrix, at least not on the length scale studied (up to 50 nm). Instead, as temperature increases, dislocations are found to aggregate, thereby forming small fluid domains. Due to the implicit entropy present in the coarse grained lipid tails, the gel phase remains untilted. Tilt, however, can be induced by a small reduction of size of the lipid tail sites.

## Acknowledgements

We thank John Nagle, Alex de Vries and Volker Knecht for careful reading of the manuscript. The research was supported by the Royal Academy of Sciences of The Netherlands (KNAW), and by the Molecule-to-Cell program of the NWO.

## References

Abraham, F.F., 1974. Homogeneous Nucleation Theory. Academic Publishing, New York.

- Berendsen, H.J.C., Postma, J.P.M., van Gunsteren, W.F., DiNola, A., Haak, J.R., 1984. Molecular dynamics with coupling to an external bath. *J. Chem. Phys.* 81, 3684–3689.
- Biltonen, R.L., Lichtenberg, D., 1993. The use of differential scanning calorimetry as a tool to characterize liposome preparations. *Chem. Phys. Lipids* 64, 129–142.
- Brannigan, G., Tamboli, A.C., Brown, F.L.H., 2004. The role of molecular shape in bilayer elasticity and phase behaviour. *J. Chem. Phys.* 121, 3259–3271.
- Chui, S.T., 1983. Grain-boundary theory of melting in two dimensions. *Phys. Rev. B* 28, 178–194.
- de Vries, A.H., Yefimov, S., Mark, A.E., Marrink, S.J. Molecular structure of the lecithin ripple phase. *Proc. Natl. Acad. Sci. U.S.A.*, in press.
- Erbes, J., Gabke, A., Rapp, G., Winter, R., 2000. Kinetics of phase transformations between lyotropic mesophases of different topology: a time-resolved synchrotron X-ray diffraction study using the pressure-jump relaxation technique. *Phys. Chem. Chem. Phys.* 2, 151–162.
- Esselink, K., Hilbers, P.A.J., van Beest, B.W.H., 1994. Molecular dynamics study of nucleation and melting of *n*-alkanes. *J. Chem. Phys.* 101, 9033–9041.
- Essmann, U., Perera, L., Berkowitz, M.L., 1995. The origin of the hydration interaction of lipid bilayers from MD simulation of dipalmitoylphosphatidylcholine membranes in gel and crystalline phases. *Langmuir* 11, 4519–4531.
- Faller, R., Marrink, S.J., 2004. Simulation of domain formation in DLPC–DSPC mixed bilayers. *Langmuir* 20, 7686–7693.
- Filippov, A., Orädd, G., Lindblom, G., 2003. The effect of cholesterol on the lateral diffusion of phospholipids in oriented bilayers. *Biophys. J.* 84, 3079–3086.
- Frenkel, J., 1946. Kinetic Theory of Liquids. Dover, New York.
- Gaede, H.C., Gawrisch, K., 2003. Lateral diffusion rates of lipid, water, and a hydrophobic drug in a multilamellar liposome. *Biophys. J.* 85, 1734–1740.
- Halperin, B.I., Nelson, D.R., 1978. Theory of two-dimensional melting. *Phys. Rev. Lett.* 41, 121.
- Hentschel, M., Miethé, P., Meyer, H., 1989. The phase diagram of 1,2-dipalmitoyl-*sn*-glycero-3-phosphocholine/sucrose in the dry state. Sucrose substitution for water in lamellar mesophases. *Biochim. Biophys. Acta* 980, 169–174.
- Kashchiev, D., 2000. Nucleation: Basic Theory with Applications. Butterworth–Heinemann, Oxford.
- Katsaras, J., Yang, D.S.C., Epan, R.M., 1992. Fatty-acid chain tilt angles and directions in dipalmitoyl phosphatidylcholine bilayers. *Biophys. J.* 63, 1170–1175.
- Kharakoz, D.P., Shlyapnikova, E.A., 2000. Thermodynamics and kinetics of the early steps of solid-state nucleation in the fluid lipid bilayer. *J. Phys. Chem. B* 104, 10368–10378.
- Kosterlitz, J., Thouless, D., 1973. Ordering, metastability and phase-transitions in two-dimensional systems. *J. Phys. C* 6, 1181.
- Koynova, R., Caffrey, M., 1998. Phases and phase transitions of the phosphatidylcholines. *Biochim. Biophys. Acta* 1376, 91–145.
- Kranenburg, M., Venturoli, M., Smit, B., 2003. Phase behavior and induced interdigitation in bilayers studied with dissipative particle dynamics. *J. Phys. Chem. B* 107, 11491–11501.

- Kuo, A.L., Wade, C.G., 1979. Lipid lateral diffusion by pulsed nuclear magnetic resonance. *Biochemistry* 18, 2300.
- Lee, B.S., Mabry, S.A., Jonas, A., Jonas, J., 1995. High-pressure proton NMR study of lateral self-diffusion of phosphatidylcholines in sonicated unilamellar vesicles. *Chem. Phys. Lipids* 78, 103–117.
- Lindahl, E., Hess, B., van der Spoel, D., 2001. *J. Mol. Model.* 7, 306–317.
- Marrink, S.J., de Vries, A.H., Mark, A.E., 2004. Coarse grained model for semi-quantitative lipid simulations. *J. Phys. Chem. B* 108, 750–760.
- Marrink, S.J., Mark, A.E., 2003. Molecular dynamics simulation of the formation, structure, and dynamics of small phospholipid vesicles. *J. Am. Chem. Soc.* 125, 15233–15242.
- Nagle, J.F., Tristram-Nagle, S., 2000. Structure of lipid bilayers. *Biochim. Biophys. Acta* 1469, 159–195.
- Orädd, G., Lindblom, G., Westerman, P.W., 2002. Lateral diffusion of cholesterol and dimyristoylphosphatidylcholine in a lipid bilayer measured by pulsed field gradient NMR spectroscopy. *Biophys. J.* 83, 2702–2704.
- Petrache, H.I., Dodd, S., Brown, M., 2000. Area per lipid and acyl length distributions in fluid phosphatidylcholines determined by H-2 NMR spectroscopy. *Biophys. J.* 79, 3172–3192.
- Quinn, R.A., Goree, J., 2001. Experimental test of two-dimensional melting through disclination unbinding. *Phys. Rev. E* 64, 051404.
- Sheats, J.R., McConnell, H.M., 1978. Photo-chemical technique for measuring lateral diffusion of spin-labeled phospholipids in membranes. *Proc. Natl. Acad. Sci. U.S.A.* 75, 4661.
- Shewchuk, J.R., 2002. Delaunay refinement algorithms for triangular mesh generation. *Comp. Geometry: Theory Appl.* 22, 21–74.
- Smit, B., Hilbers, P.A.J., Esselink, K., Rupert, L.A.M., van Os, N.M., Schlijper, A.G., 1990. Computer simulations of a water/oil interface in the presence of micelles. *Nature* 348, 624–625.
- Smith, G., Sirota, E., Safinya, C., Plano, R., Clark, N., 1990. X-ray structural studies of freely suspended ordered hydrated DMPC multilayered films. *J. Chem. Phys.* 92, 4519.
- Stevens, M.J., 2004. Coarse-grained simulations of lipid bilayers. *J. Chem. Phys.* 121, 11942–11948.
- Sun, W.J., Suter, R.M., Knewton, M.A., Worthington, C.R., Tristram-Nagle, S., Zhang, R., Nagle, J.F., 1994. Order and disorder in fully hydrated unoriented bilayers of gel phase dipalmitoylphosphatidylcholine. *Phys. Rev. E* 49, 4665–4676.
- Tieleman, D.P., Marrink, S.J., Berendsen, H.J.C., 1997. A computer perspective of membranes: molecular dynamics studies of lipid bilayer systems. *Biochim. Biophys. Acta* 1331, 235–270.
- Tu, K., Tobias, D.J., Blasie, K., Klein, M.L., 1996. Molecular dynamics investigation of the structure of a fully hydrated gel-phase dipalmitoylphosphatidylcholine bilayer. *Biophys. J.* 70, 595–608.
- Venable, R.M., Brooks, B.R., Pastor, R.W., 2000. Molecular dynamics simulations of gel phase lipid bilayers in constant pressure and constant surface area ensembles. *J. Chem. Phys.* 112, 4822–4832.
- Zhang, K.Q., Liu, X.Y., 2004. In situ observation of colloidal monolayer nucleation driven by an alternating electric field. *Nature* 429, 739–743.